FSS was designed to work at 4.2, 6, and 7 GHz with $0.13 \times 0.13\ \lambda^2$ dimensions where λ is free space wavelength at the first frequency.

REFERENCES

1. B.A. Munk, Frequency Selective Surfaces: Theory and Design, Wiley, New York, NY, 2000.
2. S.A. Winkler, W. Hong, M. Bozzi, and K. Wu, Polarization rotating frequency selective surface based on substrate integrated waveguide technology, IEEE Trans Antennas Propag 58 (2010), 1202–1213.
3. S. Chakravarty, R. Mittra, and N.R. Williams, Application of a microgenetic algorithm (MGA) to the design of broad-band microwave absorbers using multiple frequency selective surface screens buried in dielectrics, IEEE Trans Antennas Propag 50 (2002), 284–296.
4. G.I. Kiani, K.L. Ford, K.P. Esselle, A.R. Weily, and C.J. Panagamuwa, Oblique incidence performance of a novel frequency selective surface absorber, IEEE Trans Antennas Propag 55 (2007), 2931–2934.
5. A.K. Rashid, and Z. Shen, A novel band-reject frequency selective surface with pseudo-elliptic response, IEEE Trans Antennas Propag 58 (2010), 1220–1226.
6. J.C. Zhang, Y.Z. Yin, and J.P. Ma, Design of narrow band- pass frequency selective surface for millimeter wave applications, Prog Electromagn Res 96 (2009), 287–298.
7. P. Wu, F. Bai, Q. Xue, X. Liu, and S.Y. Ron Hui, Use of Frequency Selective Surface for Suppressing Radio-Frequency Interference from Wireless Charging Pads, IEEE Trans Ind Electron 61 (2014), 3969–3977.
8. Q. Chen, and Y. Fu, A Planar Stealthy Antenna Radome Using Absorber Frequency Selective Surface, Microwave Opt Tech Lett 56 (2014), 1788–1792.
9. M. Kartal, and B. Doken, A New Frequency Selective Absorber Surface at the unlicensed 2.4-GHz ISM band, Microwave Opt Tech Lett 58 (2016), 2351–2358.
10. V. Sanphuang, N.K. Nahar, and J.L. Volakis, Frequency Selective Surfaces Filters to Enhance Performance of Ka Band Application, Microwave Opt Tech Lett 56 (2014), 563–568.
11. M. Wang, C. Huang, M. Pu, and X. Luo, Reducing Side Lobe Level of Antenna Using Frequency Selective Surface Superstrate, Microwave Opt Tech Lett 57 (2015), 1971–1975.
12. M. Ohira, H. Deguchi, and M. Tsuji, Circuit Synthesis for Compact Waveguide Filters with Closely-Spaced Frequency Selective Surfaces, Int J Microwave Opt Tech 1 (2006), 366–370.
13. J. Yang, and Z. Shen, A Thin and Broadband Absorber Using Double-Square Loops, IEEE Antennas Wireless Propag Lett 6 (2007), 388–391.
14. S.E. Melais, D. Cure, and T.M. Weller, A Quasi-Yagi Antenna Backed by a Jerusalem Cross Frequency Selective Surface, Int J Microwave Sci Tech 2013 (2013).
15. M. Ohira, H. Deguchi, M. Tsuji, and H. Shigesawa, Novel Waveguide Filters With Multiple Attenuation Poles Using Dual-Behavior Resonance of Frequency-Selective Surfaces, IEEE Trans Microwave Theory Tech 53 (2005), 3320–3326.
16. Z.H. Lu, P.G. Liu, and X.J. Huang, A Novel Three-Dimensional Frequency Selective Structure, IEEE Antennas Wireless Propag Lett 11 (2012), 588–591.
17. Y. Yang, X.H. Wang, and H. Zhou, Dual-Band Frequency Selective Surface With Miniaturized Element In Low Frequencies, Prog Electromagn Res Lett 33 (2012), 167–175.
18. E.A. Parker, J.B. Robertson, B. Sanz-Izquierdo, and J.C. Batchelor, Minimal size FSS for long wavelength operation, Electron Lett 44 (2008), 1.
19. B. Sanz-Izquierdo, J.B. Robertson, E.A. Parker, and J.C. Batchelor, Wideband FSS for electromagnetic architecture in buildings, Appl Phys a 103 (2011), 771–774.
20. B. Li, and Z. Shen, Bandpass Frequency Selective Structure With Wideband Spurious Rejection, IEEE Antennas Wireless Propag Lett 13 (2014), 145–148.
21. S.M.A. Momeni Hasan Abadi, M. Li, and N. Behdad, Harmonic-Suppressed Miniaturized-Element Frequency Selective Surfaces With Higher Order Bandpass Responses, IEEE Trans Antennas Propag 62 (2014), 2562–2571.
22. C. Chiu, and W. Wang, A dual-frequency miniaturized-element FSS with closely located resonances, Antennas Wireless Propag Lett 12 (2013), 163–165.

A MIMO ANTENNA DESIGN BASED ON THE CHARACTERISTIC MODE

Jihoon Kim, Longyue Qu, Haseok Jo, Rui Zhang, and Hyeongdong Kim
Department of Electronics and Computer Engineering, Hanyang University, 17 Haengdang-dong, Seongdong-gu, Seoul, 133-791, Korea; Corresponding author: hdkim@hanyang.ac.kr

Received 20 September 2016

ABSTRACT: *In this article, multiple-input multiple-output (MIMO) antennas with high isolation and low correlation for LTE Band 8 (880–960 MHz) were designed by adopting a planar inverted-F antenna (PIFA) and a slot antenna. Based on characteristic mode theory, MIMO antennas utilize two different types of antennas to excite orthogonal modes for enhanced isolation and correlation. The proposed PIFA is designed to excite the ground mode along the length of the ground plane, and the slot antenna is proposed to adopt the ground mode along the width of the ground plane as a radiator; this provides greatly improved isolation and diversity performance compared to the reference MIMO antennas using two PIFAs. During simulation, the isolation is enhanced from below 4 to 20 dB. The measured envelope correlation coefficient (ECC) of the proposed MIMO antennas had an average value of 0.06, but the reference MIMO antennas had a very high ECC of 0.7.*
 Microwave Opt Technol Lett 59:893–898, 2017; View this article online at wileyonlinelibrary.com. DOI 10.1002/mop.30429

Key words: *MIMO antennas; high isolation; low correlation; characteristic mode*

1. INTRODUCTION

Along with the development of 4G telecommunication systems, an increase in the data transfer rate and quality of the data are highly demanded; therefore, the use of MIMO antenna systems is also increasing. In order to design a MIMO antenna system with high performance, a low correlation coefficient below 0.5 must be satisfied for mobile antennas. However, it is difficult to satisfy this condition because of strong mutual coupling between antennas that are integrated within the restricted physical area of wireless devices. A great deal of research has been performed to reduce the mutual coupling and correlation coefficient; these studies have included adding a slot [1,2] or resonator [3] in the ground plane; creating different coupling paths on the ground [4]; and adding a neutralization line or lumped circuit between antennas [5–8]. However, these studies have the common idea of inserting an additional structure for decoupling or reducing the correlation coefficient.

In this article, a method that does not add additional decoupling structures to MIMO antenna design is proposed in an attempt to enhance the isolation and the correlation performance; this is done by adopting two different types of antennas in Band 8 (880–960 MHz) applications. The reference MIMO antennas were designed by using two planar inverted-F antennas

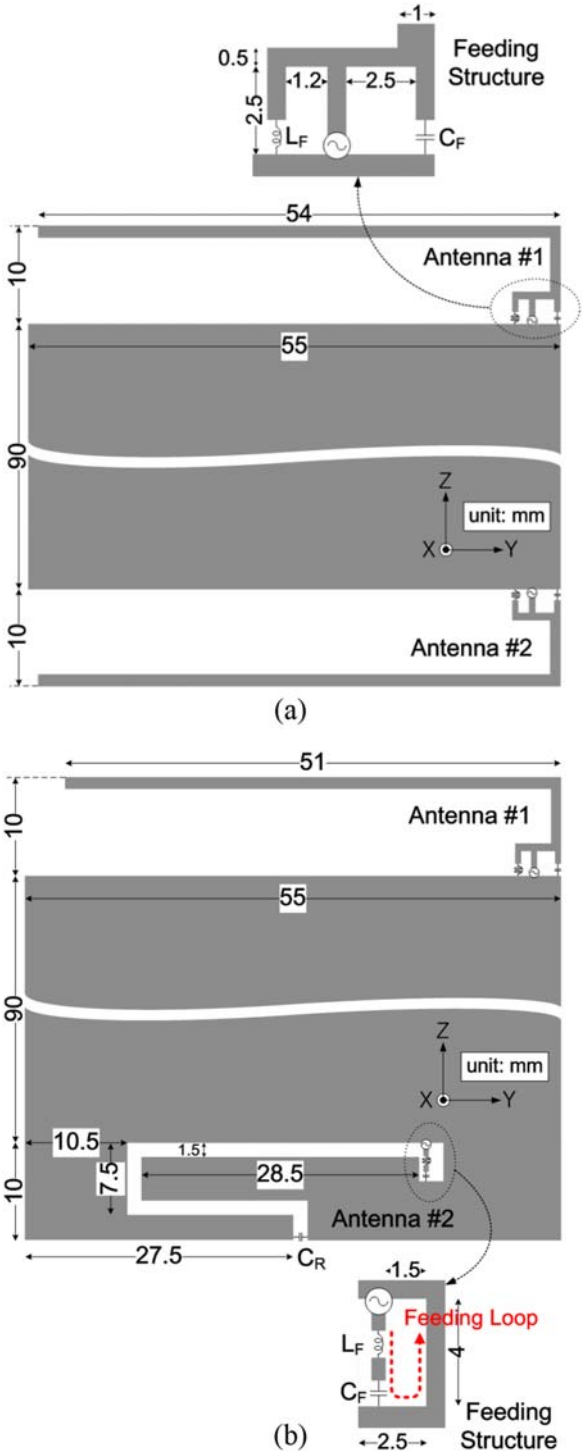

Figure 1 Geometry of the MIMO antennas: (a) the reference antennas and (b) the proposed antennas. [Color figure can be viewed at wileyonlinelibrary.com]

(PIFAs) that can adopt the same characteristic mode, resulting in high mutual coupling and poor diversity performance. The proposed antennas were designed by using a PIFA and a novel slot antenna. This allows each antenna to excite different characteristic modes that are orthogonal to each other. Therefore, the isolation and the correlation performance between the two antennas were greatly improved. In order to understand the excited characteristic modes in the reference MIMO antennas and the proposed MIMO antennas, the surface current distributions are discussed. The orthogonal modes can also be verified by analyzing the measured radiation patterns and ECC. This letter is organized as follows. In Section 2, the reference and proposed MIMO antennas are presented and the *S*-parameters are compared with each other. The operating mechanisms are analyzed in Section 3, where we explain the proposed MIMO antennas. In the last section, the measured radiation patterns and ECC results are used to verify the proposed MIMO antenna performance.

2. ANTENNA DESIGN

The configurations of the reference MIMO antennas and the proposed MIMO antennas are shown in Figure 1. About 110 mm × 55 mm printed circuit boards (PCBs) were etched on an FR-4 ($\varepsilon_r = 4.4$) with a thickness of 1 mm. As shown in Figure 1(a), the reference MIMO antennas are designed to have a PIFA at the top and bottom of the ground plane for antenna #1 and antenna #2, respectively. Each antenna occupies a clearance of 10 mm × 55 mm. The detailed dimensions are presented in Figure 1(a). To achieve easy tuning, a shunt inductor L_F (4.5 nH) and a capacitor C_F (0.7 pF) are adopted for the input impedance of each PIFA.

In Figure 1(b), the proposed MIMO antennas are designed by using a PIFA for antenna #1 and a slot-type antenna for antenna #2. To achieve a compact design within an area of 10 mm × 55 mm, the slot antenna is designed to have a C shape. Additionally, a series capacitor C_R (0.18 pF) is inserted at the open portion of the slot antenna. The resonant frequency of the slot antenna can be controlled by changing the length of the slot and/or by changing the value of the capacitor C_R without changing the length of the slot. For bandwidth consideration, the slot antenna is excited by using a series capacitor C_F (0.3 pF) and inductor L_F (63 nH). This enables wideband performance to be obtained by changing the ratio of the inductor and capacitor while keeping the resonance frequency of the feeding loop equal to the antenna operating frequency [9].

Figure 2 shows the simulated *S*-parameters of the reference MIMO antennas and the proposed MIMO antennas. In Figure 2(a), the −6 dB bandwidths of reference antenna #1 and antenna #2 are almost equal to 105 MHz (from 858 to 963 MHz), which can fully cover LTE Band 8. However, the mutual coupling S12 between antenna #1 and antenna #2 is as high as −3.9 dB, indicating poor isolation and high losses. The simulated *S*-parameters of the proposed MIMO antennas are shown in Figure 2(b), where the −6 dB bandwidths of antenna #1 and antenna #2 are 171 MHz (from 867 to 1038 MHz) and 50 MHz (from 919 to 969 MHz), respectively, which can also cover LTE band 8. It can be observed that the mutual coupling S12 for the proposed MIMO antennas is greatly reduced to −20 dB, indicating much higher isolation compared to the reference MIMO antennas. By comparison, it can be seen that the proposed MIMO antenna design can provide high isolation, even though the bandwidth is narrower.

3. OPERATING MECHANISM

It is known that the theory of characteristic modes provides new insights into mobile antenna design. The total surface current on a conducting body is the sum of all of the characteristic currents, which can be represented by the following equation [10]:

$$J = \Sigma \alpha_n J_n \tag{1}$$

Here, J is the total current and α_n represents the coefficients of each characteristic mode J_n.

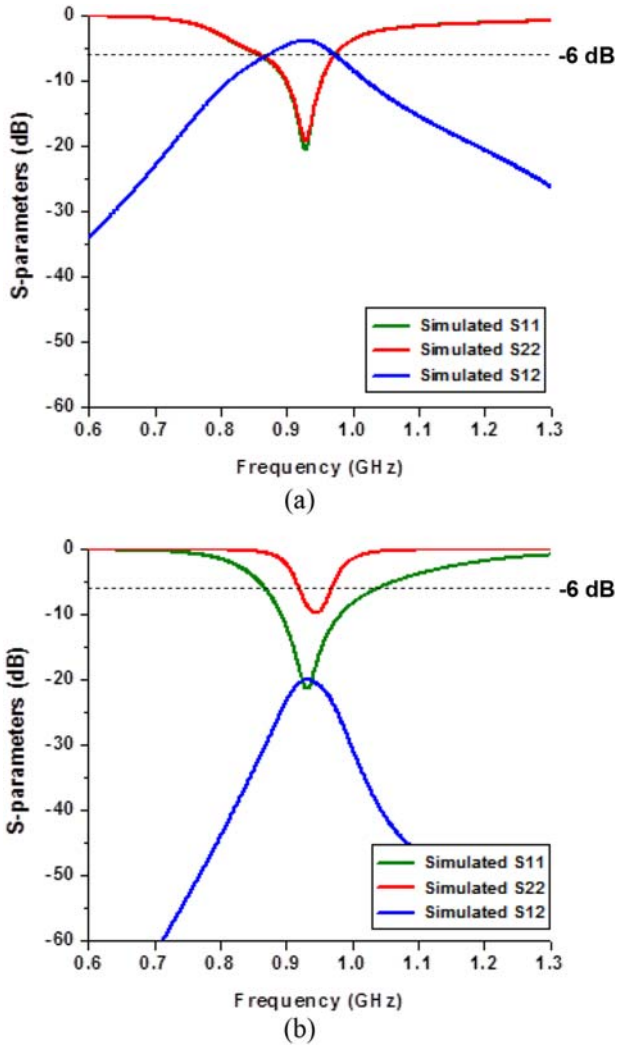

Figure 2 Simulated *S*-parameters of (a) the reference antennas and (b) the proposed antennas. [Color figure can be viewed at wileyonlinelibrary.com]

For an antenna working below the 1 GHz operating band, the ground mode along the length of the ground plane is the most promising mode for good radiation performance; this is the case because the ground mode resonance is closest to the operating frequency [11]. Another promising mode is the ground mode along the width of the ground plane; unfortunately, the resonance of this mode is much higher than the one along the length of the ground plane. In the reference MIMO antennas, both PIFAs are located at the end of the ground plane; therefore, they dominantly excite the same ground mode along the length of the ground plane for radiation, resulting in poor isolation and similar radiation patterns. Alternatively, in the proposed MIMO antennas, the slot antenna is adopted for excitation of the ground mode along the width of the ground plane and the PIFA is adopted for excitation of the ground mode along the length of the ground plane. As stated above, the slot antenna achieves narrower bandwidth performance because the ground mode resonance along the width of the ground plane is much higher than it is along the length of the ground plane. The operating principle for the ground mode excitation of the slot antenna and PIFA is provided as follows.

The coupling between the ground plane and an antenna can be expressed as:

$$<E^{g}, J^{a}> = \iiint E^{g} \cdot J^{a} d\tau \tag{2}$$

$$<H^{g}, M^{a}> = -\iiint H^{g} \cdot M^{a} d\tau \tag{3}$$

Here, E^{g} and H^{g} are the electric and magnetic fields because of the characteristic modes of the ground plane. J^{a} and M^{a} are the electric and magnetic currents generated by an antenna. According to these equations, it is obvious that electric current sources (e.g., a PIFA) are placed at the end of the ground plane where the electric field is strong. In a similar way, magnetic current sources (e.g., a slot antenna) are placed inside the ground plane where the magnetic field is strong. Two PIFAs in the reference MIMO antennas are located at the edge of the ground plane where the electric field is strong, allowing them to simultaneously excite the same ground mode. However, in the case of the proposed antenna, a PIFA is located at the edge of the ground plane; thus, it dominantly excites the ground mode along the length of the ground plane. The slot antenna mainly generates a loop current source close to the maximum magnetic field along the width of the ground plane; therefore, it excites the ground mode along the width of the ground plane.

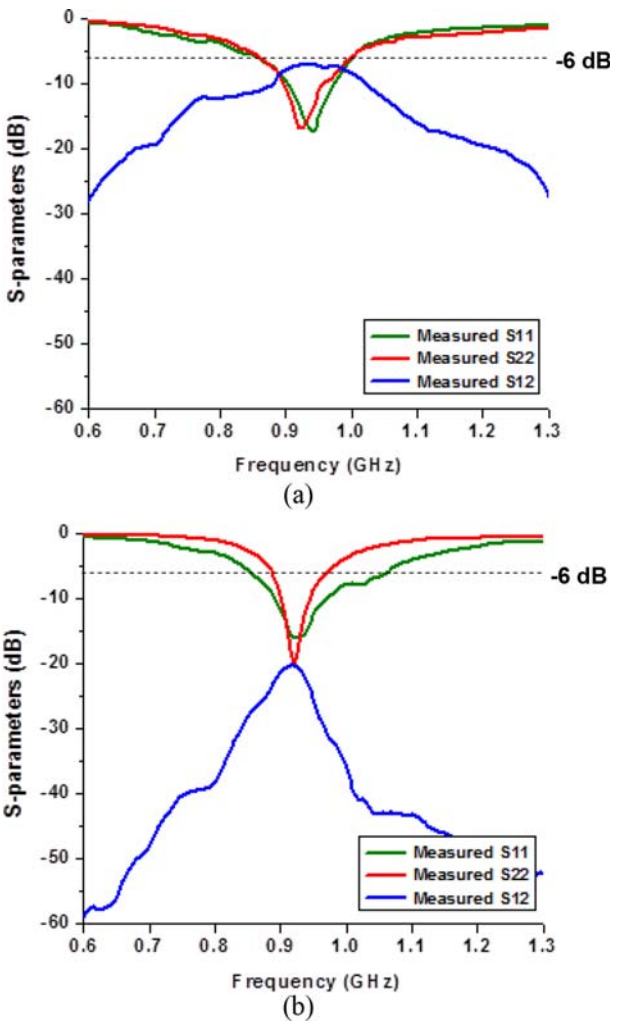

Figure 3 Measured *S*-parameters of (a) the reference antennas and (b) the proposed antennas. [Color figure can be viewed at wileyonlinelibrary.com]

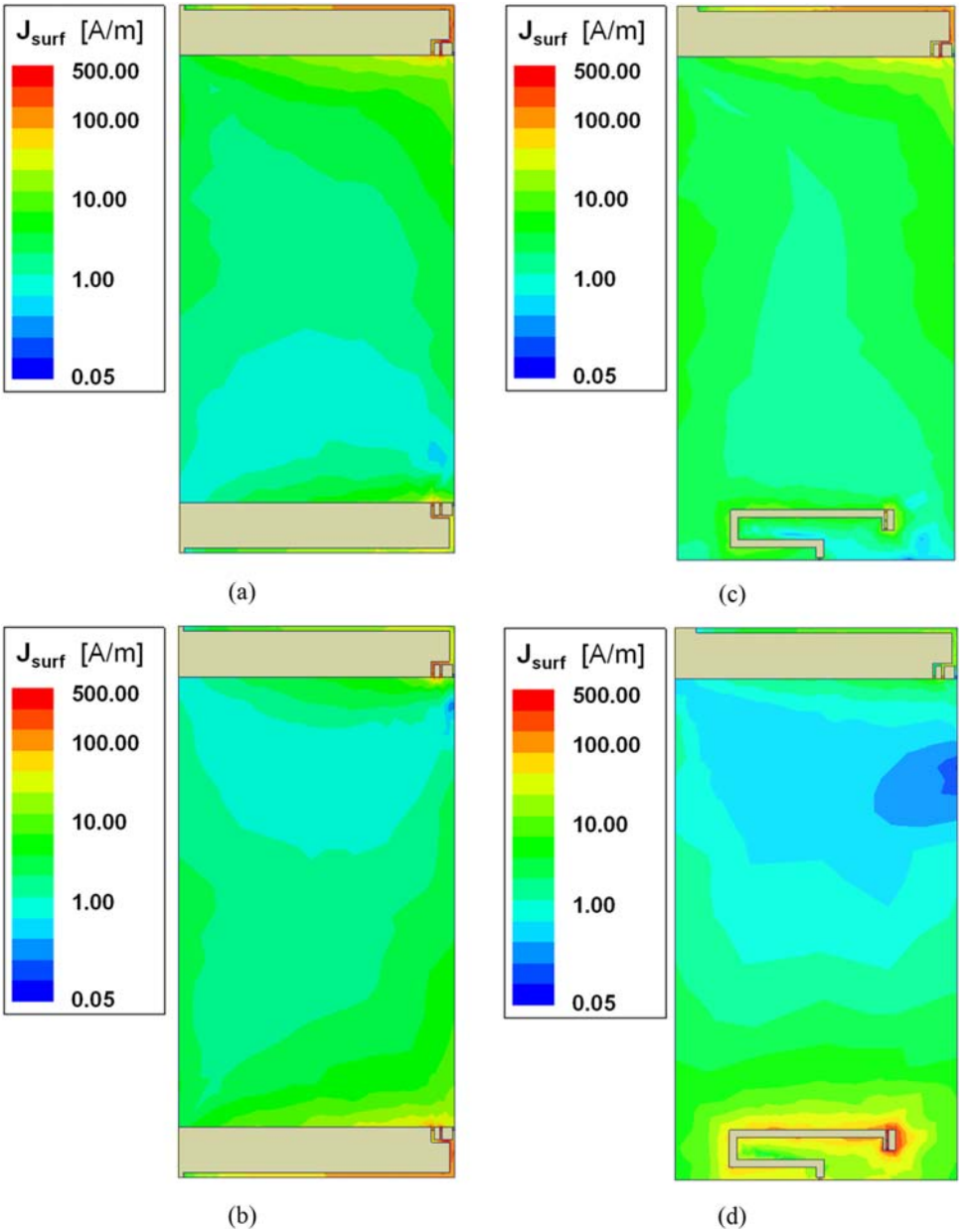

Figure 4 Simulated surface current distributions of the reference antennas ((a) with port 1 excitation and (b) with port 2 excitation) and the proposed antennas ((c) with port 1 excitation and (d) with port 2 excitation). [Color figure can be viewed at wileyonlinelibrary.com]

To verify the above analysis, the simulated surface current distributions of the reference and proposed antennas are plotted at 920 MHz in Figure 3. Figures 3(a) and [3](b) provide the surface current distributions when port 1 and port 2 are excited, respectively. Both PIFAs generate similar current distributions along the length of the ground plane (z-axis), adopting the ground mode along the length of the ground plane as a dipole-type radiator. Figures 3(c) and [3](d) show the current distributions of the proposed MIMO antenna at 920 MHz with the PIFA and the slot antenna excitation, respectively. In Figure 3(d), antenna #2 (slot antenna) generates a loop-type current distribution; this allows it to be seen as a magnetic current source along the y-axis rather than along the z-axis. Furthermore, the port-to-port induced currents from the PIFA to the slot antenna (from the slot antenna to the PIFA) are also greatly reduced because of the high isolation between the PIFA and slot antenna.

4. EXPERIMENTAL RESULTS

The reference and proposed MIMO antennas are fabricated and measured. Figure 4 shows the measured S-parameters of the reference and proposed antennas. As shown in Figure 4(a), the -6 dB bandwidths of the reference MIMO antennas are 135 MHz and the mutual coupling S12 between the two PIFAs is -7 dB. In the case of the proposed MIMO antennas, the -6 dB bandwidths of the proposed PIFA and slot antennas are 205 and 80 MHz, respectively, while the mutual coupling between the antennas is -20 dB. It can be observed that the simulation and measurement results are in good agreement with one another and have only slight differences. As stated in Section 3, two different characteristic modes that are orthogonal to each other are excited by changing the type of antenna #2 from a PIFA to a slot antenna. As a result, the mutual coupling between antenna #1 and antenna #2 can be greatly reduced.

Figure 5 illustrates the measured radiation patterns of the reference and the proposed MIMO antennas. Figure 5(a) shows the radiation patterns of reference antenna #1 and antenna #2. Both

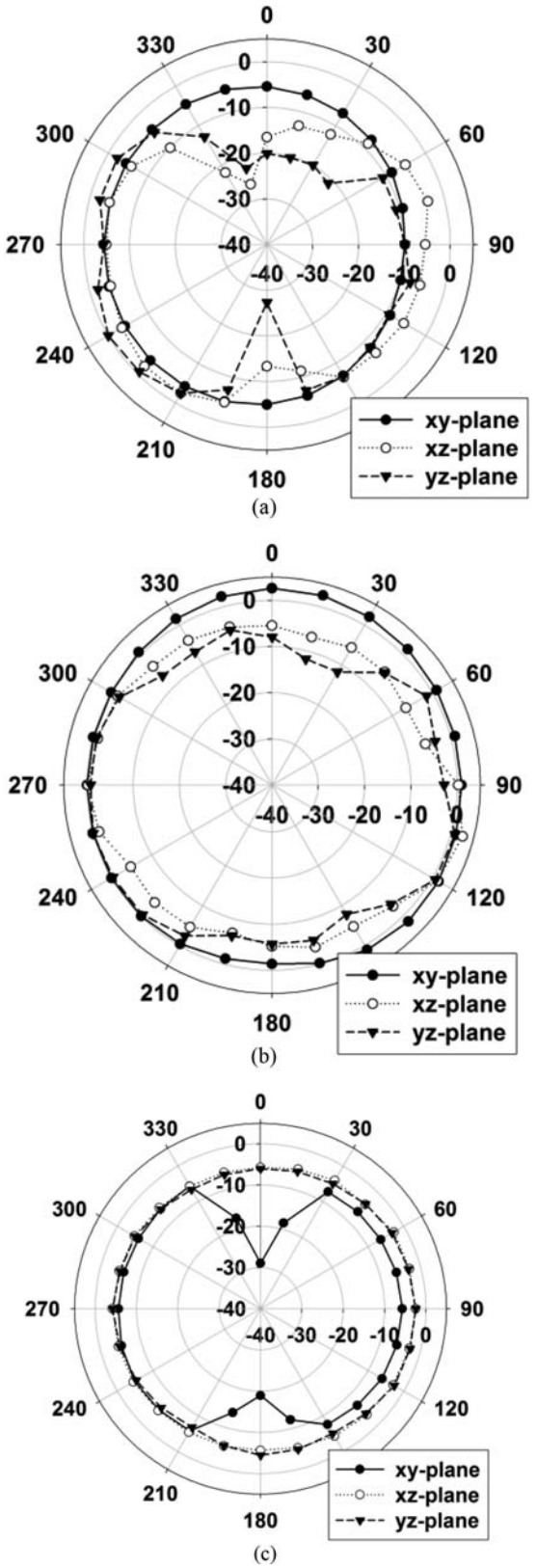

Figure 5 Measured radiation patterns of (a) the reference antenna #1 and antenna #2, (b) the proposed antenna #1, and (c) the proposed antenna #2

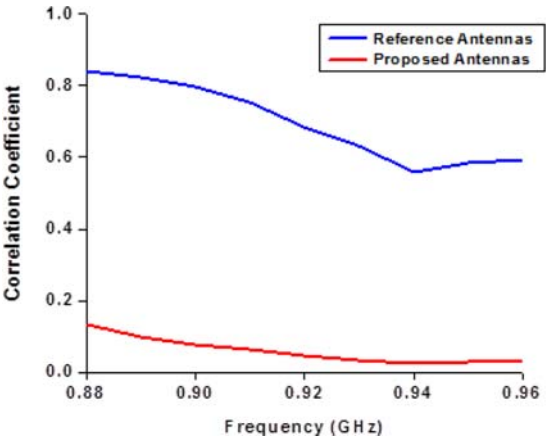

Figure 6 Measured envelope correlation coefficients of the reference antennas and the proposed antennas. [Color figure can be viewed at wileyonlinelibrary.com]

antenna #1 and antenna #2 generate similar radiation patterns since they are exciting the same ground mode. It can be seen that both antennas generate omni-directional radiation patterns in the *xy*-plane, which is coincident with the dipole-type ground mode along the *z*-axis (i.e., along the length of the ground plane). Figures 5(b) and [5](c) show the radiation patterns of the proposed PIFA and slot antenna, respectively. It can be observed in Figure 5(b) that the proposed PIFA operates as a dipole-type radiator along the *z*-axis (i.e., along the length of the ground plane). However, the proposed slot antenna generates an omni-directional radiation pattern in the *xz*-plane [depicted in Figure 5(c)], showing that the dipole-type mode along the *y*-axis (i.e., along the width of the ground plane) is excited. The characteristic mode of the antenna was changed by replacing the PIFA with a slot antenna, enabling the proposed MIMO antennas to generate orthogonal radiation patterns (as explained in Section 3).

Furthermore, to achieve good diversity performance, the ECC should be maintained below 0.5 for mobile applications. Therefore, the measured ECC values of the reference MIMO antennas and the proposed MIMO antennas are compared from 0.88 to 0.96 GHz. The measured results show that the ECCs of the reference and proposed MIMO antennas are 0.06 and 0.7, respectively. The improved ECC performance further verifies the orthogonal radiation patterns that are shown in Figure 6. The measured radiation efficiency of the reference antennas (#1, #2) and proposed antennas (#1, #2) are 43%, 43%, 62%, and 30%, respectively. As a result, the proposed technique in this letter was proven to be applicable for MIMO antennas with high isolation and low ECC.

5. CONCLUSION

In this letter, a MIMO antenna design technique is proposed to achieve high isolation and good diversity performance. In contrast to previously studied correlation performance enhancement methods, which require the addition of decoupling structures, the proposed technique is based on characteristic mode theory. The proposed PIFA and slot antenna utilize two different characteristic modes without any additional structures and obtain good diversity performance. Compared to the reference MIMO antennas using two PIFAs, the proposed MIMO antennas provide high isolation and low ECC, which has been verified by analyzing the generated orthogonal radiation patterns. The

reference and proposed MIMO antennas were designed through simulation and tested experimentally.

ACKNOWLEDGMENTS

This work was supported by the ICT R&D program of MSIP/IITP, Republic of Korea [B0101-16-1271, Ground radiation technique for mobile devices].

REFERENCES

1. M. Karaboikis, C. Soras, G. Tsachtsiris, and V. Makios, Compact dual-printed inverted-F antenna diversity systems for portable wireless devices, IEEE Antennas Wireless Propag Lett 3 (2004), 9–14.
2. G.A. Mavridis, J.N. Sahalos, and M.T. Chryssomallis, Spatial diversity two-branch antenna for wireless devices, Electron Lett 42 (2006), 266–268.Vol
3. L. Qu, R. Zhang, and H. Kim, Decoupling between ground radiation antennas with ground-coupled loop-type isolator for WLAN applications, IET Microwave Antennas Propag 10 (2016), 546–552.
4. A.C.K. Mak, C.R. Rowell, and R.D. Murch, Isolation enhancement between two closely packed antennas, IEEE Trans Antennas Propag 56 (2008), 3411–3419.
5. A. Diallo, C. Luxey, P.L. Thuc, R. Staraj, and G. Kossiavas, Study and reduction of mutual coupling between two mobile phone PIFAs operating in the DCS1800 and UMTS bands, IEEE Trans Antennas Propag 54 (2006), 3063–3074.
6. A. Diallo, C. Luxey, P.L. Thuc, R. Staraj, and G. Kossiavas, Enhanced two-antenna structures for universal mobile telecommunications system diversity terminals, IET Microwave Antennas Propag 2 (2008), 93–101.
7. Cai-Yi Lui, Yu-Shin Wang, Shyh-Jong Chung, Two nearby dual-band antennas with high port isolation, Proceedings of IEEE Antennas Propagation Society International Symposium (AP-S 2008), San Diego, CA, 2008, pp. 1–4.
8. S.-W. Su, C.-T. Lee, and F.-S. Chang, Printed MIMO-antenna system using neutralization-line technique for wireless USB-Dongle Applications, IEEE Trans Antennas Propag 60 (2012), 456–463.Vol
9. R. Zhang, Y. Liu, H. Kim, and H. Kim, PIFA using series-resonant feed structure for wide-band operations, Electron Lett 51 (2015), 606–608.Vol
10. R.F. Harrington, and J.R. Mautz, Theory of characteristic modes for conducting bodies, IEEE Trans Antennas Propag AP-19 (1971), 622–628.Vol
11. L. Qu, R. Zhang, H. Shin, J. Kim, and H. Kim, Performance enhancement of ground radiation antenna for Z-wave applications using tunable metal loads, Electron Lett, accepted

TRANSITION OF CPW TO SINRD GUIDE OF PCB VERSION

Xiaojun Hu, Fan Li, and Feng Xu

School of Electronic Science and Engineering, Nanjing University of Posts and Telecommunications, Nanjing 210003, China; Corresponding author: feng.xu@njupt.edu.cn

Received 20 September 2016

ABSTRACT: *Substrate integrated nonradiative dielectric (SINRD) waveguide fabricated directly on printed circuit board (PCB) or metalized dielectric layer, with its excellent performances of simplifying fabrication process and minimizing mechanical errors, is vitally essential at the microwave and millimeter-wave frequencies. In this article, a transition of coplanar waveguides (CPW) to the SINRD waveguides based is presented, providing effective interconnects for compactly and flexibly integrating the planar-CPW-based devices with the SINRD waveguide circuits. It is found that simulated results are in good agreements with the measured results, which proves the promising future of the SINRD waveguide of PCB version in the area of millimeter-wave hybrid integrated systems.* © 2017 Wiley Periodicals, Inc. Microwave Opt Technol Lett 59:898–900, 2017; View this article online at wileyonlinelibrary.com. DOI 10.1002/mop.30426

Key words: *CPW; millimeter-wave; PCB; SINRD; transition*

1. INTRODUCTION

Nonradiative dielectric (NRD) waveguide, since its inception in 1981 [1], has become one of the most attractive guiding structures for microwave, and in particular millimeter-wave circuits and systems. Compared to other transmission lines, NRD waveguide presents superior features of low transmission losses and almost nonexistent radiation at bends and discontinuities. However, sever problems, such as mechanical and assembly errors exist in conventional NRD waveguides. Especially when frequency increases, operating wavelength deduces, it becomes more and more difficult to implement and integrate NRD waveguide with other circuits.

To overcome the mentioned difficulties, as a development of the substrate integrated nonradiative dielectric (SINRD) waveguide in Refs. [2,3], a PCB version of SINRD waveguide has been proposed [4]. Different from the original SINRD waveguide, via-air holes or slots are drilled directly on the PCBs instead of a naked dielectric slab. To do so, a simple planar SINRD waveguide without extra metal cover is presented and subsequently the alignment problems and mechanical errors of conventional NRD waveguides can be eliminated. As a result, this type of SINRD waveguide, which is fabricated directly on PCBs or metallized layers, can be convenient to integrate with other planar circuits and corresponding, be a potential structure for future millimeter-wave hybrid integrated systems.

However, the excitation of SINRD still depends on rectangular waveguides, even if in recent applications [5,6]. As a result, it is necessary to develop a kind of planar excitation circuits because the planar transmission lines are vitally critical for millimeter-wave hybrid integrated systems. Most of the existed transitions, e.g., the transition of microstrip line to NRD waveguide and slotline to NRD waveguide [7,8], have not focused on this PCB-SINRD waveguide yet. Therefore, none of them is suitable for compact hybrid integrated circuits at higher frequencies because of the drawbacks of conventional NRD waveguides discussed before. To fulfil this void, this article proposes an integrated transition from CPW to PCB-SINRD waveguide. The simulation results demonstrate that the transition proposed perform well. Finally, measured values are also presented to compare with the simulation results. The good agreements confirm the prospects of the PCB-SINRD waveguide and its applications in the hybrid integrated system at millimeter-wave frequencies.

2. DESCRIPTION OF THE TRANSITION

So far, the hybrid integrated technology derived from the concept of the aperture coupling has been proved to be prospect in millimeter-wave systems. Figure 1 shows the electromagnetic distributions of the LSM_{11} mode in NRD waveguide. In the area of the central strip of a NDR waveguide, the electric and magnetic fields of the LSM_{11} mode can be written as

$$E_x = -A(\beta_y/\varepsilon_r)(\pi/a)\cos(\pi x/a)\sin(\beta_y y) \tag{1}$$

$$E_y = (A/\varepsilon_r)(\beta^2 + (m\pi/a)^2)\sin(\pi x/a)\cos(\beta_y y) \tag{2}$$